Growing oxide thin films in a low-energy electron microscope

Torren, A.J.H. van der

3

Low-Energy Electron Microscopy (LEEM)

Low-energy electron microscopy (LEEM) is a powerful surface science technique. It allows for real-time, in-situ imaging at elevated temperatures up to 1500°C with nanometer resolution. The surface sensitivity and large temperature window make it an ideal technique to study the formation of oxide surfaces and interfaces. In the following, I give a short introduction to LEEM and in more detail to our LEEM system called ESCHER. Furthermore, I will discuss the imaging techniques used to study the oxide interfaces.

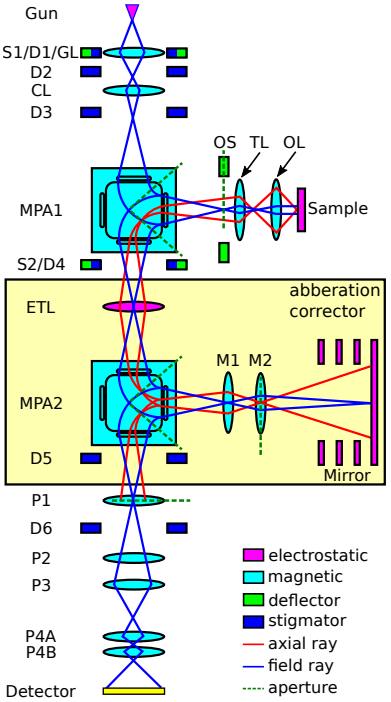

FIGURE 3.1: Schematic view of the electron-optical system of a LEEM. The yellow part is only included in the aberration corrected version. All electron-optical elements like lenses, deflectors and stigmators are labeled, and explained in the text.

3.1 Introduction to LEEM

Low-energy electron microscopy uses electrons up to 100 eV to perform surface sensitive imaging and spectroscopy. These low-energy electrons are very surface sensitive due to their low inelastic mean free path, which limits their penetration depth and is in the order of a few atomic layers [1].

Unlike scanning electron microscopes (SEM), LEEM illuminates the entire field of view at once. This allows for real-time imaging of dynamic processes. Two important components of a LEEM, are the magnetic prism array (MPA) and cathode objective lens. The MPA allows for transfer of the full field of view to the detector by separating the incoming, illuminating electrons from back-scattered electrons, used to form an image. The cathode lens is the crucial part for the low energy electrons as will be discussed later on. An illustration of the setup is shown in figure 3.1. First I will explain the non-aberration corrected version, in which the yellow part in figure 3.1 is absent.

Starting from the top, electrons leaving the electron gun are accelerated to an energy of 15 keV. These high energies are required for optimal performance of the

electron lenses. The electrons are focused by the gun lens (GL) and condenser lens (CL) and can be steered by a set of deflectors (D1-D3) before entering the magnetic prism array (MPA1), which bends the electrons by 90 ° towards the sample. After passing the transfer lens (TL) the electrons arrive at the objective lens (OL). The objective lens consists of a magnetic lens and an electrostatic lens of which the sample forms the cathode. The sample is biased with a tunable negative high voltage close to the electron gun potential of 15 kV. The strong electric field ($\approx$ 10 kV/mm) decelerates the electrons to a selected energy in the range of 0 - 100 eV. An energy of 0 eV is called mirror mode, because the electrons just start to turn around before any interaction happened, and the sample becomes a mirror. After interaction with the sample, the electrons will be accelerated back to 15 keV in the same electric field. A diffraction pattern or in general the angular distribution of the electrons, is formed at the back focal plane of the objective lens and further along, a real-space image is formed at the image plane in the center of the magnetic prism array. To clarify the optical path, the field (blue) and axial (red) rays are drawn into figure 3.1. The axial or marginal ray starts at the point where the object crosses the optical axis and ends at the aperture stop. This ray crosses the optical axis at all points where an image is made. The field ray is parallel to the optical axis at the object and crosses the optical axis at the back focal plane.

Once the electrons are back at the prism array MPA1, it deflects the electrons downwards into the projector column. The projector column with lenses P1-4, magnifies and transfers the image onto the detector. Fast switching between imaging and diffraction mode is possible by turning on lens (P2) in the projector column. The lenses P4A-B can be used as a rotation free doublet for low magnifications or as a telescope for very strong magnification. The detector is build up out of a micro-channel plate, phosphor screen and camera. The channel plate amplifies the signal my multiplying the incoming electrons. The outgoing electrons are converted to photons with a phosphor screen, the photons are detected by a camera.

3.2 Aberration-corrected LEEM

The ESCHER (Electronic, Structural and CHEmical nanoimaging in Real-time) machine is the LEEM system located at Leiden University. It is based on the aberration corrected FE-LEEM P90 instrument (SPECS GmbH, Berlin) designed by Tromp[2,3]. The advantage of an aberration corrected LEEM is an increased spatial resolution up to 1.4 nm, a world record for LEEM, which was measured on this machine. The resolution of a LEEM machine is limited by the chromatic and spherical aberrations induced by the cathode objective lens OL. While these aberrations cannot be corrected by lenses since electron lenses can only be convex, the lowest order aberrations can be corrected by an electrostatic mirror[4]. The mirror is built up out of three high voltage rings, allowing for three degrees of freedom in the mirror shape. The voltages can be chosen such that the chromatic and spherical aberrations are opposite to the ones induced by the cathode lens while the mirror back plane stays in focus. The mirror is incorporated into the LEEM

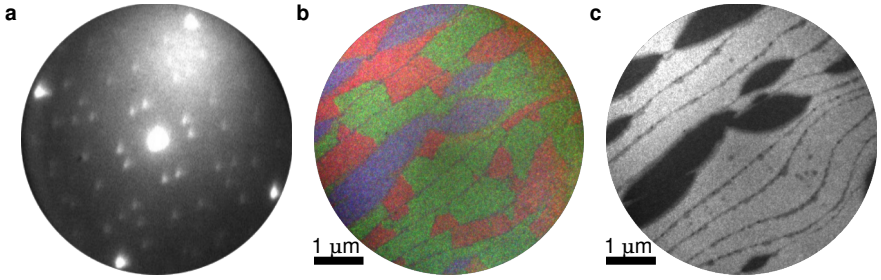

FIGURE 3.2: a) A LEED pattern of mixed terminated $SrTiO_3$ sample, taken at 14 eV. On the edge the four bright diffraction spots of the cubic perovskite unit cell can be seen while the spots around the center are from two rotations of the $\sqrt{13} \times \sqrt{13}$ R33.7 surface reconstruction. The spots of the 2×2 surface reconstruction are very vague. b) A multi darkfield image taken at 12 eV, red and green are the two rotations of the $\sqrt{13} \times \sqrt{13}$ R33.7 surface reconstruction while the blue area is 2×2 reconstructed. c) A bright field image taken at 12 eV of the same sample. The 2×2 reconstructed area is dark. Also the step edges are dark, due to destructive interference or phase contrast.

by introducing a second magnetic prism array (MPA2, Fig. 3.1). An electrostatic transfer lens (ETL) is placed between the two prisms to invert the image without rotations such that the dispersion of the two prisms cancel. An extra set of lenses (M1/M2) is placed between MPA2 and mirror to create a rotation-free defocused image on the mirror, optimizing the mirror performance.

3.3 Standard imaging techniques

A low energy electron microscope offers a unique opportunity in sample analysis by combining many measurement techniques. In the following sections I will briefly describe the main techniques used.

3.3.1 Low-energy electron diffraction (LEED)

The driving force behind many of the imaging techniques ina LEEM is the opportunity to combine real-space imaging with diffraction experiments. For electrons, crystalline samples will act as a grating and a diffraction pattern in the far field is the result. This technique is called low-energy electron diffraction (LEED) An example is shown in figure 3.2a of a $SrTiO_3$ crystal annealed at 1200 °C in air for 12 hours. The annealing leads to a mixed terminated surface with areas of TiO_2 and SrO areas [5,6]. On the edge of the image, bright spots are seen in a square pattern, the square surface net of $SrTiO_3$. In the center the specular spot represents the electrons scattered back perpendicular to the surface. The other spots are a combination of a $\sqrt{13} \times \sqrt{13}$ R33.7 surface reconstruction, with different directions, and a 2×2 reconstruction. The $\sqrt{13} \times \sqrt{13}$ R33.7 surface reconstruction is known to exists on the TiO_2 terminated part [7]. The 2×2 reconstruction is likely to be caused by SrO termination [5,6].

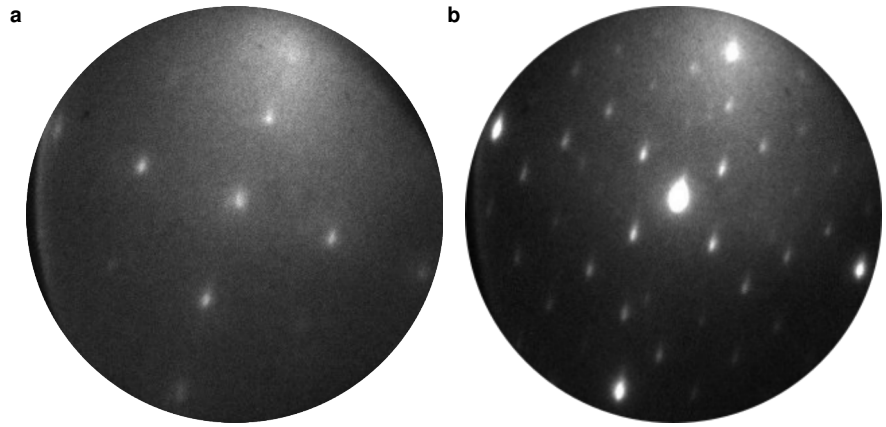

FIGURE 3.3: μLEED images of a mixed terminated $SrTiO_3$ sample. a) Taken at the 2×2 reconstructed part, blue in figure 3.2b. b) One of the two rotations of the $\sqrt{13} \times \sqrt{13}$ R33.7 reconstructed part. Both images are taken at 14 eV.

3.3.2 Bright field & dark field LEEM and μLEED

As stated earlier the strength of LEEM is combining real-space and diffraction information. By placing an aperture around one of the diffraction spots, the areas contributing to this spot can be imaged in real-space. An example is shown in figure 3.2b where three images are merged by adding them in red, green and blue. For every color in the image a diffraction spot of one of the three surface reconstructions is selected. The spots of the two rotations of the $\sqrt{13} \times \sqrt{13}$ R33.7 reconstruction are selected for red and green while a spot of the 2×2 reconstruction is selected for blue. In the results we can clearly see the diffraction patterns originate from distinct areas of the surface.

One can also select the center or specular diffraction spot. The real-space image now shows contributions of two effects. In the first place the intensity at a given energy is related to the (electronic) structure as will be described in more detail in section 3.4.4. This can be observed in figure 3.2c, where the intensity is different on the TiO_2 and SrO terminated areas. A second effect originates from the wave nature of the electrons. The electron waves can cause destructive interference at the step edges, for specific energies of the incoming electrons. This produces dark lines as shown in figure 3.2c and is called phase contrast.

Not only a part of the diffraction image can be selected, but also a part of a real-space image. The aperture now selects only a small region on the sample and the reconstruction on this region can be imaged. This is demonstrated in figure 3.3, where figure 3.3a is taken on a TiO_2 terminated area and figure 3.3b on a SrO terminated area of the $SrTiO_3$ sample. This technique is called micro-LEED (μLEED).

3.3.3 LEEM-IV

More quantitative data can be obtained from a diffraction pattern by not only collecting the position of the diffraction spots, but also the intensity dependence on the landing energy (or sample voltage) of the electrons. These are so called LEED-IV curves and can be used as a fingerprint or be compared with calculations of a model system. Compared to standard LEED the energies used in LEEM are even lower. This is sometimes called very low energy electron diffraction or VLEED. In this range multiple scattering is less important and for the specular diffraction spot, the data are close to the unoccupied band structure[8,9]. In LEEM this method can be extended with spatial resolution by selecting the specular diffraction spot with an aperture and image the real space IV-curve[10].

3.3.4 Photoemission electron microscopy (PEEM)

By turning off the electron beam and illuminating the sample with UV light the machine can be changed to a photoemission electron microscope (PEEM). Although this is an interesting technique in itself, in this thesis it is mainly used for alignment and as a localization technique. The spot of the electron beam is around 5 µm while the UV light illuminates the full sample so that images of a few hundred microns can be made.

3.4 Extending the possibilities

For the investigation of electronic and growth properties of perovskites like $SrTiO_3$ and $LaAlO_3$, a low-energy electron microscope is very suitable. It can perform real-time imaging while allowing for the high measurement temperatures required for the growth of these oxide materials. However, many other components still had to be added. In the following section I will explain more about the extensions we developed for the study of perovskite growth. First of all, the hardware: pulsed laser deposition (PLD), preparation chamber, heating laser (including laser safety). However, these days a complex measurement machine cannot be controlled without software and long and repeatable growth experiments cannot be achieved without automation. To achieve the automation a flexible software system has been developed.

Furthermore, the layer-by-layer growth of the perovskites studied in this thesis requires imaging techniques not commonly used in LEEM. Section 3.4.3 will introduce spot-profile analysis LEED (SPA-LEED). Improving the technique of angle-resolved reflection electron spectroscopy (ARRES) developed in our group allowed for repetitive probing of the electronic structure as will be explained in section 3.4.4.

3.4.1 Hardware

First of all, a pulsed laser deposition (PLD) system was added for the growth of perovskites. This PLD setup is described in chapter 5. Besides the PLD system the machine has also been equipped with a preparation chamber where in combination

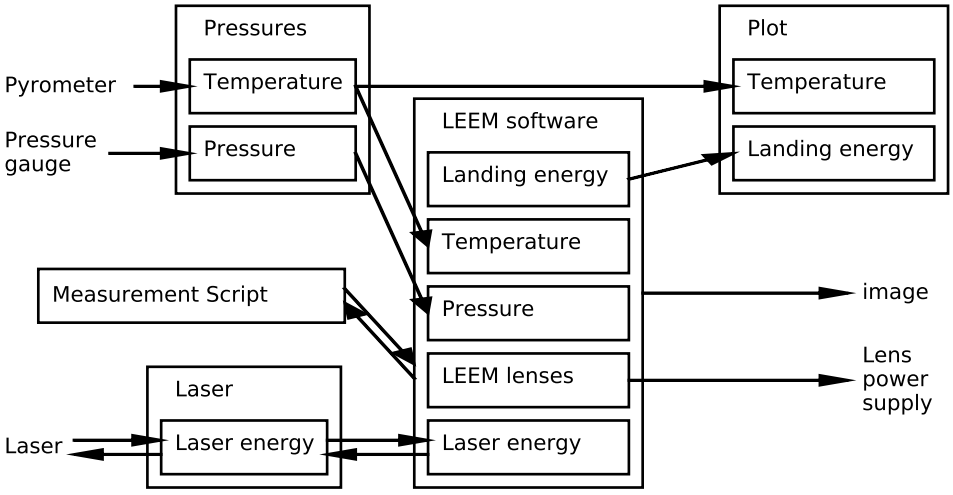

FIGURE 3.4: Example of data flow between software programs.

with a 100 W, 808 nm diode laser, the perovskite samples can be annealed in high oxygen pressures. This laser heater can also be attached to the main sample chamber to serve as an alternative for the electron bombardment heater. I developed a flexible interlock system enabling the heater to be used in combination with or next to the pulsed laser deposition system in both sample and preparation chamber while the machine is standing in an open experimental hall.

3.4.2 Software

Long repeatable growth processes require logging of growth parameters during the process as well as automatic control of the equipment. For this, new software has been developed. Figure 3.4 shows a flow diagram of the software programs and the data flows between them.

The existing LEEM software consists of a database containing all the electron lens values. These values can be controlled from the software as well as via a network transparent protocol. The program has been changed to extend the communication protocol and to save the database to the header of every image in order to have a complete description of the 'machine state' at the time the image was taken. Furthermore, the database can be extended with new variables via the communication protocol.

In order to flexibly add new hardware, a python program has been written, accommodating a parallel database containing the state of equipment around the machine. This program uses the network interface to communicate with the main LEEM program in order to exchange necessary data. The image acquisition time of the order of 100 to 250 ms only requires to push the data a few times a second. The advantage of this parallel database is flexibility for extension without loss of

stability or the need to restart the LEEM control software. Figure 3.4 shows a program 'pressures' which reads the pressure gauge and temperature and pushes it to LEEM software. The program writes to a log file to support plotting of temperature and pressure independent of imaging.

On the fly hardware changes are required when changing from standard LEEM to pulsed laser deposition (chapter 5) or other new developments like potentiometry[11] or eV-TEM[12]. For the hardware control the communication protocol is extended with a callback function. When the callback function is enabled, the LEEM software sends a signal to the python program when the variable is changed. The python software can then communicate the change to the hardware. Figure 3.4 also shows a 'Laser control' program communicating back and forth to the hardware, and the LEEM software.

Once the basic protocols are in place, extra features can be added like a plotting script which can now communicate to our python server as well as directly to the LEEM software to plot for example the electron landing energy or sample temperature.

Measurement automation scripts can use the same protocol to communicate to LEEM software. For this purpose the communication protocol has been further extended. In the first place one would like to stop and test scripts without the risk of ending up in an unwanted machine state, where possibly the alignment of the microscope is lost. To accommodate this, variables have to be locked when a script it started. When a variable is locked, the value is stored and when the connection to the measurement script is lost, the value is restored to its original state. Moreover, collision between scripts is avoided by allowing only one script to change a variable.

3.4.3 Spot-profile-analysis LEED (SPA-LEED)

Measurement automation allows for new measurement techniques. One of these techniques is spot-profile-analysis low-energy electron diffraction (SPA-LEED). In SPA-LEED we use the fact that the diffraction pattern yields more information than only the intensity and position of the diffraction spots, which results in crystal structure information. By analyzing the shape of the diffraction spots we can learn about the surface roughness. This is an important analysis for layer-by-layer growth, where the surface roughens when a layer starts to grow and flattens when a full layer has been grown.

An example is shown in figure 3.5 for the specular diffraction spot. Here figure 3.5a shows the intensity versus energy (LEED-IV-curve) and figure 3.5b shows two example spot profiles at 40 eV (red) and 75 eV (green, dashed). This SPA-LEED technique is not so commonly used in combination with LEEM. An important reason is the change in intensity of the reflected electrons in the order of 10^4 when scanning the energy as can be seen in figure 3.5a. This large range of intensities make it impossible to resolve the spot shape over the full range, with a camera of only 12-bit image depth.

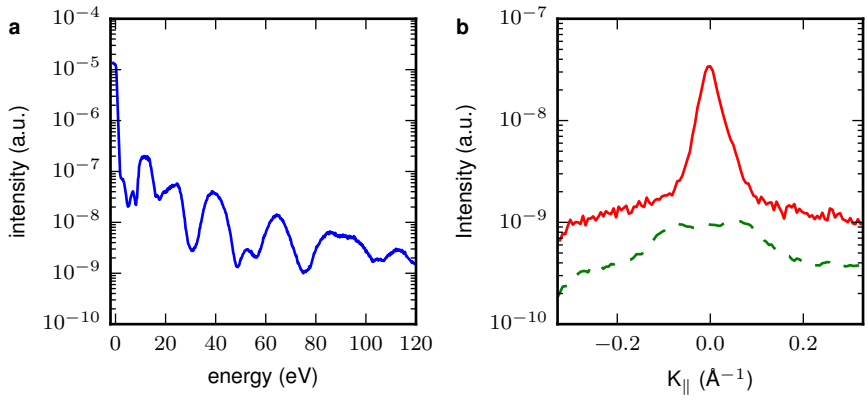

FIGURE 3.5: a) Maximum specular spot intensity versus energy for 1/2 unit cell homo-epitaxial $SrTiO_3$. b) Spot profile for the same sample at 40 eV (red) and 75 eV (green, dashed). $K_{\parallel}$ is the in-plane wave vector of the electrons forming the diffraction spot.

To gain enough image depth for the images shown in figure 3.5, a method was developed to automatically adjust the gain of our imaging system, keeping the maximum intensity on the camera around 75% of its maximum. As described before, the imaging system here is a microchannel plate detector which multiplies the incoming electrons. The outgoing electrons are converted to photons with a phosphor screen, the photons are finally detected by the camera. The gain of the channel plates can easily be adopted by changing the amplification voltage. We characterized this gain to follow $I = (I_{cmr} - b)e^{-GV_{cp}}$, where I_{cmr} is the intensity measured by the camera, b the background signal originating from the camera readout noise, V_{cp} is the voltage over the channel plates in kV, G is the gain and I is the final intensity. Here the gain was measured to be 20 kV^{-1}. In practice the channel plate voltage V_{cp} lies between 0.9 kV and 1.7 kV resulting in a six orders of magnitude amplification range.

For a so-called high-dynamic range energy scan, automatic adjustment of the gain is implemented in the energy scan script by calculating the gain required for 75% saturation of the camera after each image. This gain is used to capture the next frame. Expecting a smooth and slowly changing brightness, the intensity of the next image will thus lie within range of the camera.

For real-time growth analysis the high-dynamic range scans are automatically analyzed and time versus full-width-half-max (FWHM) of the specular diffraction spot is plotted to analyze the growth.

3.4.4 Angle-resolved reflection electron spectroscopy (ARRES)

Parallel to my work Johannes Jobst and Jaap Kautz developed a technique to probe the unoccupied band structure of graphene[9] in our LEEM setup. In this technique the intensity of the specular spot is measured as function of the energy and in-plane momentum of the electrons. In first order the signal depends on the availability of a state in the material with the same energy and in-plane momentum $k_{\parallel}$ as the electron. If this state is available the electron will couple into the material, otherwise it will reflect.

This measurement can be done in diffraction, where one averages the signal over a 5 micron spot, as well as in real-space where an aperture is used around the specular spot and full spatial resolution can be obtained. I improved this technique and made it easy to use for quick and repetitive measurements by adding high dynamic range as well as full automation of the measurement. For automation of real-space ARRES it is important to not only change the parallel momentum $k_{\parallel}$ of the electron by changing deflector D1 (Fig. 3.1), but also to keep the imaged area constant by correcting any beam shift by D3. Furthermore, the aperture in the diffraction plane has to be moved due to the displacement of the specular spot in the diffraction plane when $k_{\parallel}$ is changed.

References

[1] S. Tanuma, C. J. Powell, and D. R. Penn, *Calculations of electron inelastic mean free paths. V. Data for 14 organic compounds over the 502000 eV range*, Surface and Interface Analysis **21**, 165 (1994).

[2] R. Tromp, J. Hannon, A. Ellis, W. Wan, A. Berghaus, and O. Schaff, *A new aberration-corrected, energy-filtered LEEM/PEEM instrument. I. Principles and design*, Ultramicroscopy **110**, 852 (2010).

[3] R. Tromp, J. Hannon, W. Wan, A. Berghaus, and O. Schaff, *A new aberration-corrected, energy-filtered LEEM/PEEM instrument II. Operation and results*, Ultramicroscopy (2013).

[4] S. M. Schramm, J. Kautz, A. Berghaus, O. Schaff, R. M. Tromp, and S. J. van der Molen, *Low-energy electron microscopy and spectroscopy with ES-CHER: Status and prospects*, IBM Journal of Research and Development **55**, 1:1 (2011).

[5] R. Bachelet, F. Snchez, F. J. Palomares, C. Ocal, and J. Fontcuberta, *Atomically flat SrO-terminated $SrTiO_3$(001) substrate*, Applied Physics Letters **95**, 141915 (2009).

[6] R. Bachelet, F. Snchez, J. Santiso, C. Munuera, C. Ocal, and J. Fontcuberta, *Self-Assembly of $SrTiO_3$(001) Chemical-Terminations: A Route for Oxide-Nanostructure Fabrication by Selective Growth*, Chemistry of Materials **21**, 2494 (2009).

[7] D. M. Kienzle, A. E. Becerra-Toledo, and L. D. Marks, *Vacant-Site Octahedral Tilings on* $SrTiO_3$ *(001), the* $(\sqrt{13} \times \sqrt{13})R33.7^\circ$ *Surface, and Related Structures*, Physical Review Letters **106**, 176102 (2011).

[8] V. N. Strocov, H. I. Starnberg, P. O. Nilsson, H. E. Brauer, and L. J. Holleboom, *New Method for Absolute Band Structure Determination by Combining Photoemission with Very-Low-Energy Electron Diffraction: Application to Layered* VSe_2, Physical Review Letters **79**, 467 (1997).

[9] J. Jobst, J. Kautz, D. Geelen, R. M. Tromp, and S. J. van der Molen, *Nanoscale measurements of unoccupied band dispersion in few-layer graphene*, Nature Communications **6**, 8926 (2015).

[10] J. B. Hannon, J. Sun, K. Pohl, and G. L. Kellogg, *Origins of Nanoscale Heterogeneity in Ultrathin Films*, Physical Review Letters **96**, 246103 (2006).

[11] J. Kautz, J. Jobst, C. Sorger, R. M. Tromp, H. B. Weber, and S. J. van der Molen, *Low-Energy Electron Potentiometry: Contactless Imaging of Charge Transport on the Nanoscale*, Scientific Reports **5** (2015).

[12] D. Geelen, A. Thete, O. Schaff, A. Kaiser, S. J. van der Molen, and R. Tromp, *eV-TEM: Transmission electron microscopy in a low energy cathode lens instrument*, Ultramicroscopy **159**, 482 (2015).